2.3 Atomic Physics

2.3.1 Polarization of 1s- and 2s- electrons in highly stripped O-ions emerging from magnetized thin Ni-layers

S. Kremeyer [a], K.-H. Speidel [a], H. Busch [a], U. Grabowy [a], J. Cub, G. Jakob, P. Maier-Komor, J. Gerber [b], A. Meens [b]

[a] Institut für Strahlen- und Kernphysik, Universität Bonn

[b] Centre de Recherches Nucléaires, Strasbourg, France

Swift ions emerging from magnetized ferromagnetic layers into vacuum carry substantial electron polarization. Its magnitude is correlated with the polarization of the ions while traversing the ferromagnet leading to the well known transient magnetic fields (TF)[1].

In former measurements, the degree of polarization of 1s- and 2s- electrons (p_{1s},p_{2s}) of ^{16}O-ions emerging from magnetized Fe- and Gd- layers has been determined using a plunger setup for the time differential technique[2, 3]. In addition, the degree of polarization of ions emerging from magnetized Ni- layers has been measured as well[4]. Whereas only for Ni as ferromagnet, the observed p_{1s}- value was in good agreement with that obtained from TF- measurements, for Fe and Gd only half the polarization acquired inside these ferromagnets was preserved on emergence into vacuum. This behaviour is attributed to the presence of a cleaner surface of the Ni- layers in comparison to Fe and Gd.
Here we report on further measurements of the degree of polarization for single 1s- and 2s- electrons of ^{16}O- ions emerging from magnetized Ni- layers. The larger accuracy for the p_{2s}- value was obtained by choosing a lower ion velocity leading to a larger fraction of Li- like ions with the relevant 2s- electrons. Moreover, present measurements included plunger distances with higher sensitivity to the polarization of 2s- electrons, which were not investigated in the former experiments.

Targets consisted of a rolled and well stretched 700 $\mu g/cm^2$ thick Ti- foil implanted with ^{4}He on one side, while on the other side a 220 $\mu g/cm^2$ thick Ni- layer was deposited. Since the deposition was done as a last step of the target preparation, the Ni- surface could be kept very clean. Due to the high temperature (473 K) applied during the deposition, which was necessary to obtain good ferromagnetic behaviour, only half of the implanted He could be retained in the target. The Ni- foil was well magnetized by an external field of 0.03 T.

The ^{16}O(3^-) state ($E_\gamma = 6.13\ MeV$, $\tau = 26.6\ ps$, $g = 0.556(4)$) was populated in the inverse ^{4}He(^{16}O, α) reaction at a 44 MeV ^{16}O- beam yielding the large anisotropy $W(30°)/W(65°) = 12.3(3)$ for the unperturbed angular correlation of the ^{16}O($3^- \rightarrow 0^+$) γ- transition. A stretched 16.6 mg/cm^2 thick Ta- foil served as stopper for the ^{16}O- ions emerging from the target at a mean velocity of $v_{ion} = 6.7\ v_0$ ($v_0 = c/137$). The plunger distance d was varied between 4 and 150 μm corresponding to phase angles from $\omega_{1s}t \approx \pi/8$ to 5π, whereby ω_{1s} is the hyperfine frequency of the 1s- electron. This range of plunger distances included phase angles close to $\omega_{2s}t = \pi/2$, at which the sensitivity to the polarization of 2s- electrons is maximum. It is noted, that the hyperfine frequencies ω_{2s}^H ($(2s)^1$,H-like) and ω_{2s}^{Li} ($(1s)^2(2s)^1$,Li-like) are approximately ten times smaller than ω_{1s}.

The perturbed angular correlation depends in general on both the ion fractions with specific electron configurations and their degree of polarization which can be determined in suitable experimental conditions (see [2]).

In order to determine the degree of polarization, it was necessary to know the relevant ion fractions of the lower ion velocity ($v_{ion} = 6.7v_0$). This was achieved by measuring the anisotropy $W(30°)/W(65°)$ as a function of plunger distance (Figure 1). As expected, at the lower velocity, the fraction of H- like ions was smaller and the fraction of Li- like ions larger compared to the data at the higher velocity (Table 1).

	H-like		He-like			Li-like
electron configuration	(1s)^1	(2s)^1	(1s)^1(2s)^1	(1s)^1(2p)^1		(1s)^2(2s)^1
spectroscopic term	$^2S_{\frac{1}{2}}$	$^2S_{\frac{1}{2}}$	$^3S_1$	$^3P_1$	$^3P_2$	$^2S_{\frac{1}{2}}$
$v_{ion} = 6.7v_0$	27(3)	3(3)	5(4)	0(1)	5(3)	13(6)
$v_{ion} = 7.2v_0$	32(1)	3(3)	7(1)	0(1)	10(1)	9(3)

Table 1: Normalized fractions of electron configurations relevant to the observed hyperfine interactions

The degree of polarization results in an asymmetry of the angular correlation with respect to the beam direction. It was measured at sensitive angles of γ- detectors and plunger distances by changing the magnetization direction of the Ni- layer. The magnitude can be extracted from the ratios

$$DR(d) \quad := \quad \frac{N_1\uparrow}{N_1\downarrow} \Big/ \frac{N_2\uparrow}{N_2\downarrow} \;=\; \left(\frac{W_{exp}(\Theta_\gamma)}{W_{exp}(-\Theta_\gamma)}\right)^2$$

$$\sim \quad p_{1s}q_{1s}\cdot\sin(\omega_{1s}\cdot d/v) + p_{2s}q_{2s}^{H}\cdot\sin(\omega_{2s}^{H}\cdot d/v) + p_{2s}q_{2s}^{Li}\cdot\sin(\omega_{2s}^{Li}\cdot d/v)$$

where N_1 and N_2 are counting rates measured by detectors placed at angles symmetric to the beam axis ($\Theta_\gamma = \pm 55°$) and the arrows ($\uparrow\downarrow$) refer to opposite directions of the external field; q_{1s} and q_{2s} are the fractions of this relevant electron configurations. A best fit to the data displayed in Figure 1 yielded for the polarization of 1s- and 2s- electrons the values:

$$p_{1s} = 0.034(5) \qquad \text{and} \qquad p_{2s} = 0.061(49)$$

As already found for Fe and Gd, a substantial polarization of 2s- electron configurations is obtained. It is noted, that for all three ferromagnetic materials, the degree of 2s- polarization is consistently larger than for 1s- electrons, which is also expected from spin exchange model calculations [5]. Assuming that the ratio of polarization between 1s and 2s does not depend on the ferromagnetic species, the average obtained is

$$p_{2s}/p_{1s} = 2.3(4)$$

As the (DR-1) value for infinite plunger distance depends mainly on the polarization of 2s- electron configurations, time integral measurements are in progress to improve the present accuracy of the data.

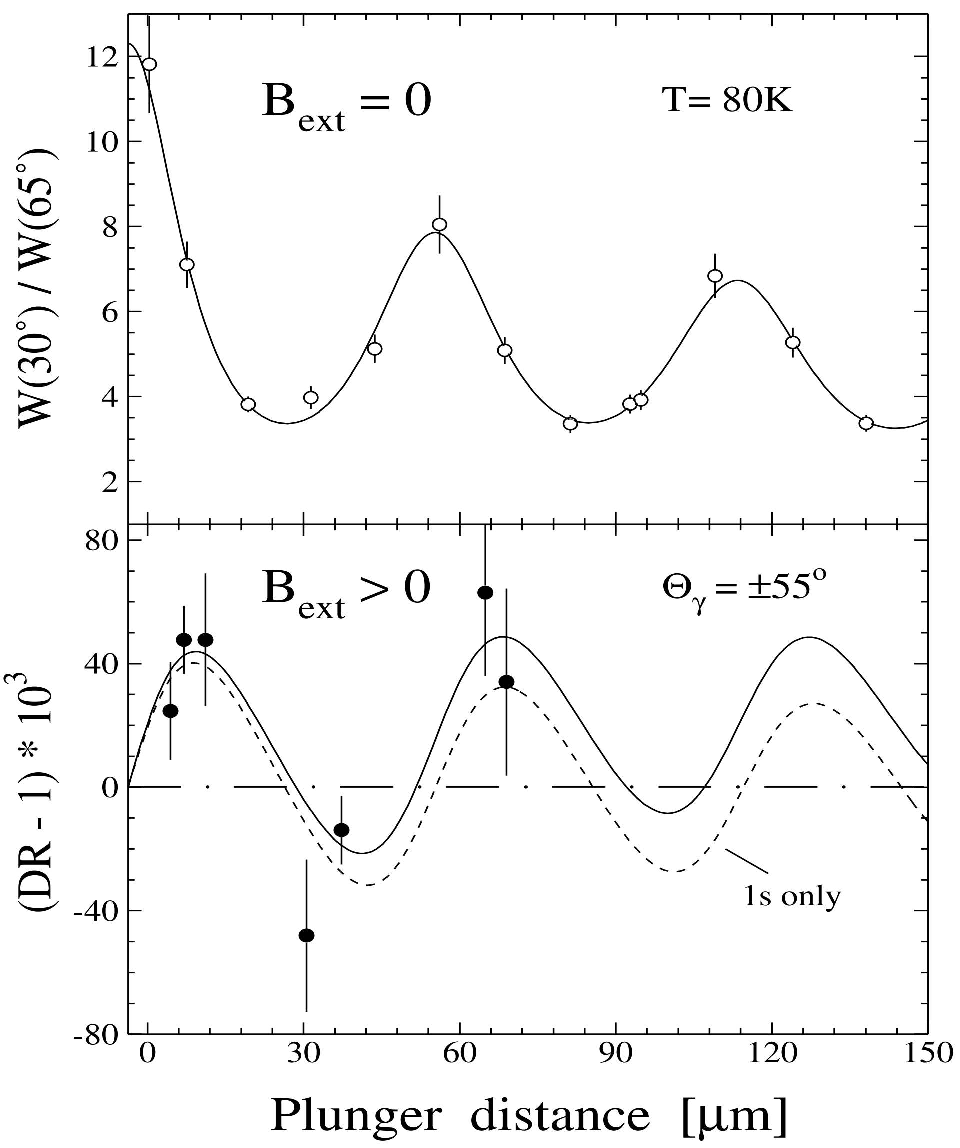

Fig. 1: Anisotropies and counting rate ratios for 'up-down' directions of the external field versus plunger distance. Solid lines are least squares fits to the data implying specific ion fractions (see table) and polarizations of 1s- and 2s- electrons. Dashed curve refers to 1s- electrons only (see text).

[1] K.-H. Speidel et al., Phys. Rev. Lett. **61** (1988) 2616

[2] H.-J. Simonis et al., Phys. Lett. **254B** (1991) 35

[3] S. Kremeyer et al., Jahresbericht 1991, p.77

[4] S. Kremeyer et al., Jahresbericht 1990, p.61

[5] F.Hagelberg et al., Z. Phys. **D17** (1990) 17 and to be published

2.3.2 Stopping power dependence of transient magnetic fields in Fe- and Gd-hosts using ^{48}Ti- and ^{79}Br-beams

G. Jakob, J. Cub, R. Pröls, K.-H. Speidel [a], H. Busch [a], S. Kremeyer [a], U. Grabowy [a], J. Gerber [b]

[a] Institut für Strahlen- und Kernphysik, Universität Bonn

[b] Centre de Recherches Nucléaires, Strasbourg, France

Transient magnetic fields (TF) act at nuclei of swift ions passing through polarized ferromagnetic solids. Their magnitude lies in the region of several kT. The phenomenon of TF is linked to the polarization of electrons in singly occupied ns-states of the ions. That polarization is transferred by spin-exchange scattering of the polarized 3d- or 4f-electrons of the ferromagnet with the unpaired ns-electrons of the moving ion. Thus, the microscopic nature of TF can be described as an effective hyperfine field, whose strength reaches maximum values for H-like ions, due to the large Fermi contact fields of 1s-electron.

In general (not only for H-like systems) the dependence of TF strengths is well described by an empirical linear parametrization formula [1]:

$$B_{TF}^{lin} = a(host) \cdot Z_{ion} \cdot \frac{v_{ion}}{v_0}, \tag{13}$$

where Z_{ion} is the atomic number of the ion in question, v_{ion} its velocity in the ferromagnetic host and $v_0 = c/137$ the Bohr-velocity. The strength parameter a depends on the host, with $a(Fe) = 12T$ and $a(Gd) = 17T$.

In various measurements of TF on light and medium-heavy nuclei it was found that the ion beams used for generating the probe ions can substantially reduce the effective fields. These TF attenuations can be expressed by the ratio between the measured TF and its expected value according to the linear parametrization (1):

$$G = \frac{B_{TF}^{exp}}{B_{TF}^{lin}}; \tag{14}$$

In those works it was found, that TF attenuations show a completely uncorrelated behaviour between beam- and probe-ions and furthermore, depend on the specific energy loss $\frac{dE}{dx}$ of the beam ions in the ferromagnetic layer [2, 3].

As can be seen from data in Fe-host (Fig. 1) a threshold for the TF attenuations appears at $\frac{dE}{dx} \approx 8\ \frac{MeV}{\mu m}$. The data show a tendency of further attenuations with an increase of $\frac{dE}{dx}$ above this threshold. The difference in the TF reductions observed for different probe ions at the same dE/dx values is attributed to the polarization of the specific electron state of the probe ions: the 3s-electron state is evidently less affected than the 1s-electron state. This particular feature has been supported by measurements on the same probe ion by varying the electron state via ion velocity [4].

Up to date all measurements give a fundamental signature of dynamic perturbations of the ferromagnetic solids. These perturbations in question diminish the electron polarization available for the TF at the probe ion.

Investigating the $\frac{dE}{dx}$-curves in Gd-hosts, especially at $\frac{dE}{dx} \approx 8\ \frac{MeV}{\mu m}$ and higher values, ^{48}Ti- and ^{79}Br-beams with energies of 120 MeV and 215 MeV, respectively, were applied to ferromagnetic gadolinium. In a target layer of Mg or Si preceding the Gd- layers (see Table 1) these and the corresponding projectiles were Coulomb excited.

The TF precessions of these probe states in the Gd-layer were measured using the perturbed particle-γ-angular correlation technique. Experimental details are given in [5]. Double ratios DR of counting rates were measured with two pairs of γ-detectors.

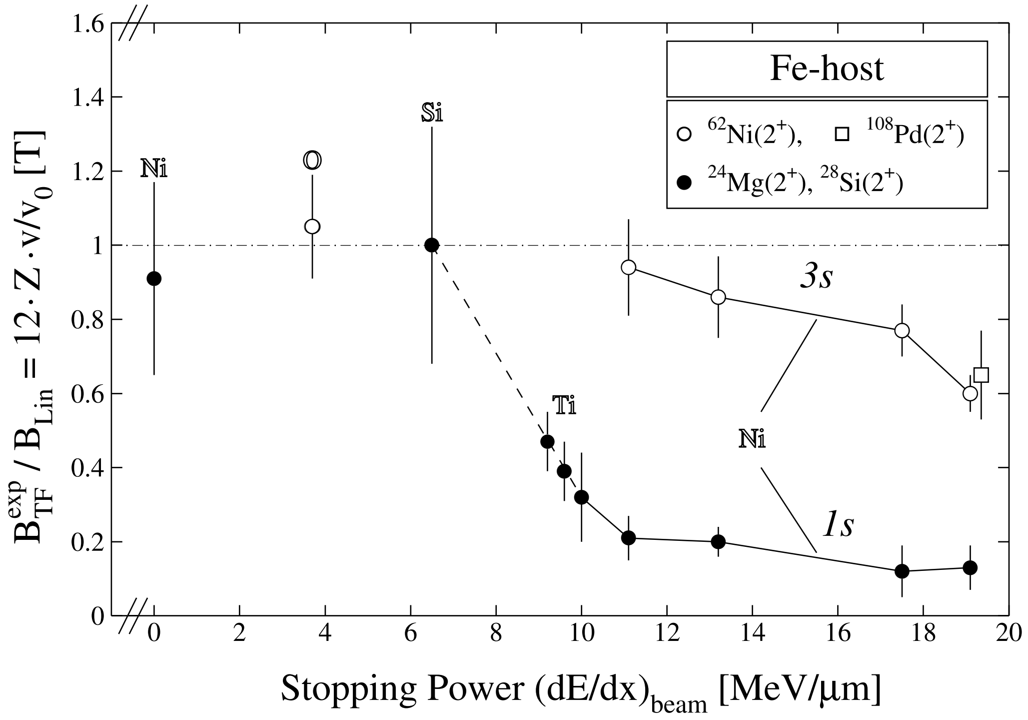

Fig. 1: TF ratios for various probe ions (see insert) versus the stopping power of beam ions in Fe host (marked at data points). The electron nature of TF is assigned. The lines are to guide the eye.

For small precession angles ϕ can be expressed as:

$$\phi = \frac{\sqrt{DR}-1}{\sqrt{DR}+1} \cdot \left(\frac{1}{W} \cdot \frac{dW}{d\Theta}\right)^{-1} = g \cdot \frac{\mu_N}{\hbar} \cdot B_{TF} \cdot t_{eff}, \qquad (15)$$

where $W(\Theta)$ refers to the angular correlation; t_{eff} being the effective interaction time of the probe ions in the ferromagnet and g the g-factor of the probe state. With the known g-factors for the 2^+-states of ^{48}Ti, ^{24}Mg and ^{28}Si B_{TF} values were determined (eq.(3)). The attenuation factors G (eq. (2)) deduced are presented in Fig. 2 as a function of $\frac{dE}{dx}$ of the corresponding beam ions. Previously measured data employing Si-, S-, Fe- and Ni-beams have also been added.

From the data of H-like ions (1s-TF), it can be seen, that a threshold for the TF attenuation is less pronounced in Gd than in Fe and appears at lower $\frac{dE}{dx}$-values. Furthermore, a significant decrease of the TF with increasing stopping power in the ferromagnet is visible. Similar to Fe-host the TF of heavier slow ions (3s-TF) show smaller reduction.

beam	Mg $[\frac{mg}{cm^2}]$	Gd $[\frac{mg}{cm^2}]$	Ta $[\frac{mg}{cm^2}]$	Cu $[\frac{mg}{cm^2}]$
^{48}Ti	1.1	11.1	1.0	1.2
^{48}Ti	1.2	7.2	1.0	1.3

beam	Si $[\frac{mg}{cm^2}]$	Gd $[\frac{mg}{cm^2}]$	Ta $[\frac{mg}{cm^2}]$	Al $[\frac{mg}{cm^2}]$
^{79}Br	0.85	4.4	1.0	1.4

Table 1: Composition of multi-layered targets

The relevant quantities of the two experiments described are summarized in Table 2.

Probe state	fields	$<\frac{v_{ion}}{v_0}>$	$<B_{TF}^{exp}>$ [T]	t_{eff} [fs]	G	$<\frac{dE}{dx}>_{beam}$ $[\frac{MeV}{\mu m}]$
$^{24}Mg(2^+)$	1s	9.9	1350(110)	530	0.67(5)	6.6
$^{48}Ti(2^+)$	3s	0.81	360(40)	1060	1.11(11)	6.6
$^{24}Mg(2^+)$	1s	10.7	1360(120)	340	0.62(6)	8.4
$^{48}Ti(2^+)$	3s	0.75	320(30)	980	1.01(8)	8.4
$^{28}Si(2^+)$	1s	13.8	1080(260)	150	0.33(8)	15.5

Table 2: Results with ^{48}Ti- and ^{79}Br-beams

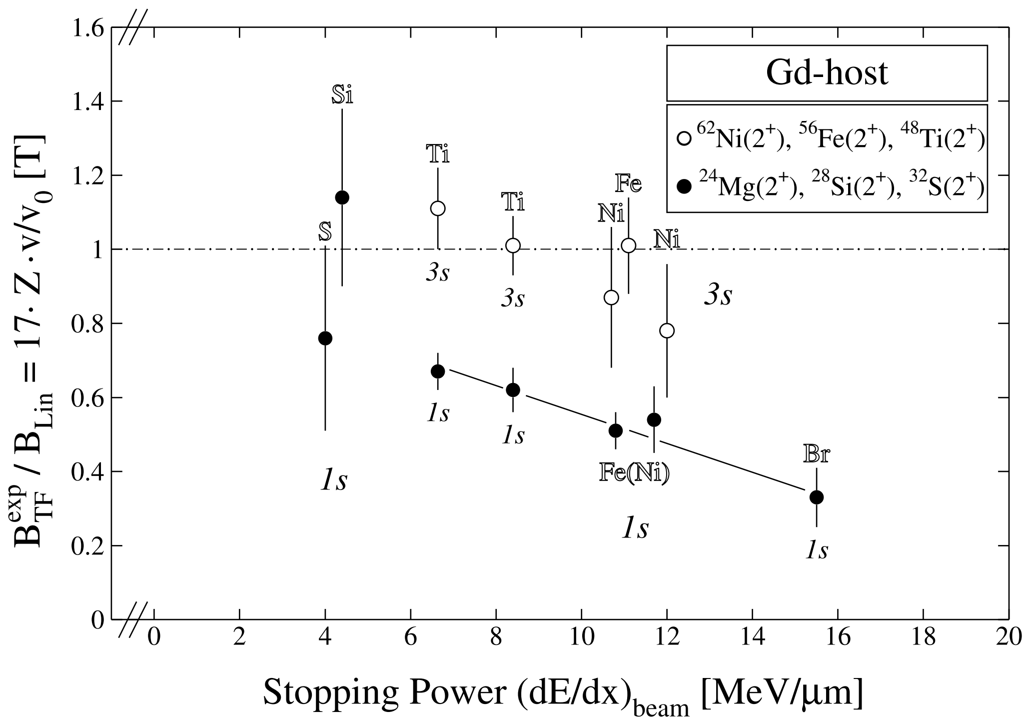

Fig. 2: TF ratios and assignments as in fig. 1 for Gd host.

[1] N. Benczer-Koller et al., Ann. Rev. Nucl. Part. Sci. **30** (1980) 53
[2] K.-H. Speidel et al., Phys Lett. **227B** (1989) 16
[3] K.-H. Speidel et al., Mat. Sci. Forum **97-99** (1992) 615
[4] K.-H. Speidel et al., Z. Phys. **D22** (1991) 371
[5] Jahresbericht 1989, 63

2.3.3 Search for transient electric field gradients in H-like ^{32}S ions

J. Cub, M. Bussas, W. Karle, U. Knopp, K.-H. Speidel [a], H. Busch [a], H.-J. Wollersheim [b], J. Gerl [b], K. Vetter [b], C. Ender [c], F. Köck [c], J. Gerber [d]
[a] Institut für Strahlen- und Kernphysik, Universität Bonn,
[b] GSI Darmstadt,
[c] Max-Planck-Institut für Kernphysik, Heidelberg,
[d] Centre de Recherche Nucléaires, Strasbourg, France

A large electric field acts on ions during the slowing down in a solid [1]. This "wake field" is induced by the interaction of the ion's positive charge with the electrons of the solid and can be understood as cause for the energy loss of the ions. The associated field gradient is predicted to have a sharp peak with typical values of

$$\frac{\partial E_z^{wake}}{\partial z} := V_{zz}^{wake} \sim 10^{17}\frac{\mathrm{V}}{\mathrm{cm}^2}$$

at the position of the ion moving in z-direction [2]. Moreover, V_{zz}^{wake} is expected to deform the electron cloud of the ion and enhance the field gradient at the nucleus by some orders of magnitude, similar to the "Sternheimer effect" in the case of static field gradients.

As the well-known transient magnetic fields, these transient electric field gradients are expected to reach their maximum values at the Bohr velocity of the 1s-electron $v_{ion} \sim Z \cdot v_0$ ($v_0 = c/137$), where the ions are predominantly hydrogenlike. A rough estimate of an upper limit for the field gradients caused by K-shell electrons, showing a strong Z-dependence, is given by [3]

$$V_{zz}^{TEFG} = \frac{16eZ^3}{27a_0^3} \approx 6.4 \cdot Z^3 \cdot 10^{17}\frac{\mathrm{V}}{\mathrm{cm}^2} \quad , \tag{16}$$

where a_0 is the "Bohr radius". For field gradients of $V_{zz}^{TEFG} \sim 10^{22}\frac{\mathrm{V}}{\mathrm{cm}^2}$, the interaction with the quadrupole moment of nuclear states with lifetimes $\tau \sim 1$ ps could be measured via the PAC technique, which would be a new method to measure quadrupole moments of short-lived states.

Up to now, there is no experimental evidence for the transient electric field gradient, but upper limits were deduced for ^{24}Mg-ions in Mg ($V_{zz}^{TEFG} \leq 10^{21}\frac{\mathrm{V}}{\mathrm{cm}^2}$) [3] and ^{148}Nd-ions in Pb ($V_{zz}^{TEFG} \leq 4 \cdot 10^{19}\frac{\mathrm{V}}{\mathrm{cm}^2}$) [2]. The latter experiment, however, was performed with multi-electron ions. This situation was strong motivation for a detailed investigation of the particle-γ-angular correlation measured in a transient field experiment with hydrogenlike ^{32}S [4] at $v_{ion} \approx 16v_0$, because of the large quadrupole moment of the first excited state of $Q(^{32}S(2_1^+)) = -16(2)\mathrm{fm}^2$. The experiment had been done at the MPIK Heidelberg by Coulomb excitation of 260 MeV ^{32}S- projectiles on a Ta/Gd-target with thicknesses of 1 mg/cm^2 and 10 mg/cm^2, respectively.

In general, the angular correlation of the γ-rays in the rest frame of the decaying nucleus can be expressed by [5]

$$W(\Theta_\gamma, \Phi_\gamma - \Phi_p) = \sum_{k,k',q,q'} F_k \cdot Q_k \cdot G_{k'k}^{q'q\,*} \cdot \varrho_{k'q'} \cdot Y_{kq}^*(\Theta_\gamma, \Phi_\gamma - \Phi_p) \quad , \tag{17}$$

where F_k are the correlation coefficients, Q_k the correction for finite solid angles, $G_{k'k}^{q'q}$ the time integrated perturbation coefficients, ϱ_{kq} the statistical tensor [6] of the observed nuclear state, $\Theta_{p,\gamma}$ and $\Phi_{p,\gamma}$ the polar and azimuthal angles of the scattered particles and deexcitation γ-rays, respectively.

At first, a fit to the Φ-dependence of the angular correlation (see Fig. 1) was done, assuming an isotropic perturbation with independent $G_k = G_{k'k}^{q'q} \cdot \delta_{k'k} \cdot \delta_{q'q}$, yielding

$$G_2^{exp} = 0.88(5) \quad \text{and} \quad G_4^{exp} = 0.89(4) \quad .$$

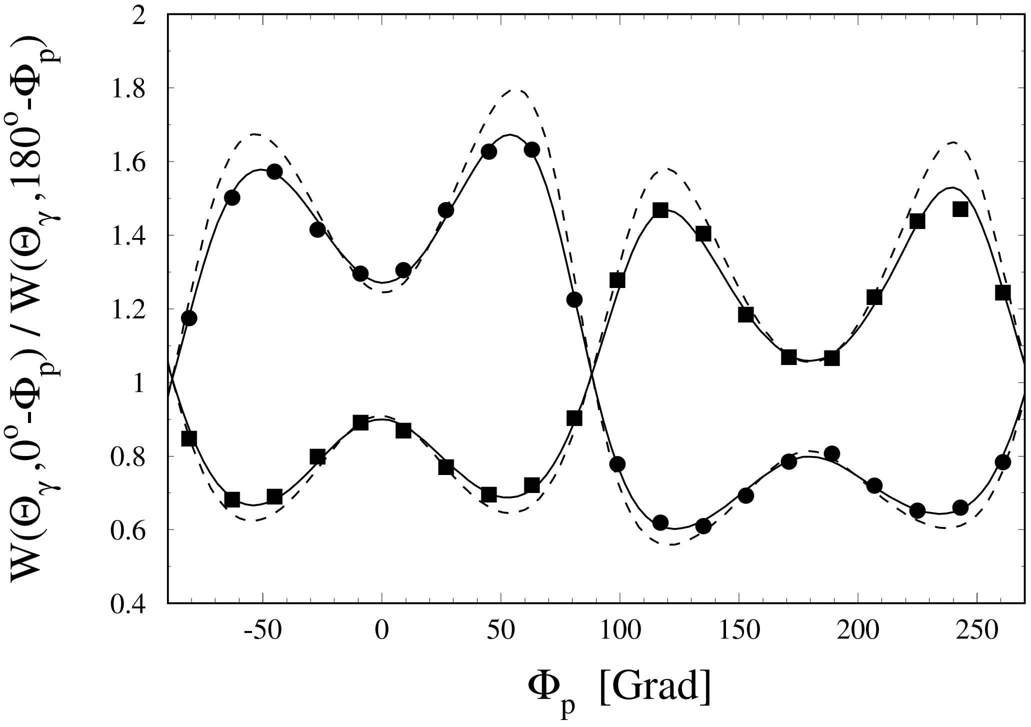

Fig. 1: ^{32}S-γ-angular correlation measured with Φ_p-position-sensitive particle counter as the ratio of two pairs of Ge-detectors ($\Phi_\gamma = 0°, 180°$) at $\Theta_\gamma^{lab} = 31°$ (quadratic symbols) and $\Theta_\gamma^{lab} = 136°$ (circles). The statistical errors are of less or equal size than the symbols. The full line is a least squares fit to the data as explained in the text while the dashed line shows an unperturbed correlation.

Such an interaction is present due to the hyperfine coupling in the ^{32}S-ions recoiling into vaccum. At the ion's velocity of emergence of $v_{ion} \approx 14 v_0$, an amount of $q_{1s} = 0.40$ is in a hydrogenlike state. This fraction is reduced to an effective value of $q_{1s}^* = 0.13$, because 67% of the ^{32}S(2_1^+)-nuclei decay inside the target. For these ions with $J = \frac{1}{2}$ one expects [7]

$$G_k = 1 - q_{1s}^* \cdot \frac{k(k+1)}{(2J+1)^2} \cdot \frac{(\omega_{1s}\tau)^2}{1+(\omega_{1s}\tau)^2} \tag{18}$$

where the hyperfine frequency ω_{1s} of a 1s-electron is given by

$$\omega_{1s} = (2J+1) \cdot g \cdot \frac{\mu_N}{\hbar} \cdot B_{1s} \quad . \tag{19}$$

With $B_{1s} = 70$ kTesla and $g = 0.50(3)$ being the nuclear g-factor of ^{32}S(2_1^+). One obtaines

$$G_2^{calc}(J = \tfrac{1}{2}) \;=\; 0.97 \quad \text{and} \quad G_4^{calc}(J = \tfrac{1}{2}) \;=\; 0.92 \quad .$$

Inclusion of further perturbations by heliumlike ion fractions in excited configurations (e.g. $J = 1$) yields

$$G_2^{calc}(J = \tfrac{1}{2}, J = 1) \;=\; 0.96 \quad \text{and} \quad G_4^{calc}(J = \tfrac{1}{2}, J = 1) \;=\; 0.88 \quad ,$$

which is close to the observed values but cannot explain the equality of G_2^{exp} and G_4^{exp}.

To account for the possible interaction of the quadrupole moment of ^{32}S(2_1^+) with a transient electric field gradient during the transit time through the Ta/Gd-target of ~ 0.3 ps, the general perturbation coefficents $G_{k'k}^{q'q}$ were calculated according to [5]. In addition to the magnetic hyperfine interactions in vacuum the best fit yielded for the field gradient the value

$$V_{zz}^{TEFG} = 2(2) \cdot 10^{21} \frac{\mathrm{V}}{\mathrm{cm}^2}$$

This result is consistent with the maximum expectation value (eq. 1) of

$$V_{zz}^{TEFG} = 2.5 \cdot 10^{21} \frac{\mathrm{V}}{\mathrm{cm}^2} \quad .$$

The large error of V_{zz}^{TEFG} is attributed to uncertainties in the angle positions of the γ- and particle-detectors of $\approx 1°$. It is noted that the experiment was not especially designed to measure transient electric field gradients. Nevertheless, ^{32}S(2_1^+) seems to be a suitable candidate for such experiments, because a reduction of the systematic errors would decrease the total error to the level of the statistical uncertainty which is by a factor of 5 lower.

[1] Z. Vager et al., Phys. Rev. Lett. **37** (1976) 1352
[2] W. Korten et al., Z. Phys. **A339** (1991) 217
[3] H. Ernst et al., Phys. Rev. **C26** (1982) 2039
[4] J. Cub et al., Jahresbericht 1991, p. 80 and Z. Phys. **A**, in press
[5] R.M. Steffen, K. Alder, in "The electromagnetic interaction in nuclear spectroscopy", ed. W.D. Hamilton, (North Holland 1975) p. 583
[6] A. Winther, J. de Boer, in "Coulomb excitation", ed. K. Alder and A. Winther (Acad. Press 1966) p. 303
[7] G. Goldring, in "Heavy ion collisions", ed. R. Bock, (North Holland 1982) Vol. 3, p. 483

2.3.4 Segmented ferromagnetic targets for transient field measurements

P. Maier-Komor, A. Stolarz, J. Cub, G. Jakob, R. Pröls, K.-H. Speidel [a], H. Busch [a], S. Kremeyer [a], U. Grabowy [a], A. Meens [b], J. Gerber [b]
[a] Institut für Strahlen- und Kernphysik, Universität Bonn,
[b] Centre de Recherche Nucléaires, Strasbourg, France

Transient magnetic fields which act on nuclei of fast moving ions in ferromagnetic solids are a unique tool to measure magnetic moments of short-lived nuclear states. Accelerated ion beams are required both to excite the probe state and to obtain high velocities of the probe ions [1].

In detailed investigations it was found that the observed field strength can be significantly reduced if heavy ion beams are employed. This is attributed to dynamic perturbations of the ferromagnetism, if the specific energy loss dE/dx of the beam ions to the electrons of the ferromagnet exceeds a critical value [2].

The experimental results indicate long lateral ranges of the order of 100 μm for the perturbation caused by a single particle hit and a characteristic recovery time for the ferromagnetic alignment of $\leq 1\mu$s. A striking idea was to use targets with magnetically decoupled segments with sizes of $\sim 10\mu$m, to restrict the perturbation to a smaller area. In this configuration the attenuations of transient magnetic fields are expected to be less pronounced. Such targets have been prepared by vaccum evaporation of iron through suitable mesh masks of 4 μm thickness and 3.05 mm in diameter, which are normally used as frames for electron transmission microscopy. The meshes had tetragonal and hexagonal shapes with a width of 50 μm. During deposition the mask joined closely the aluminium backing foil. A special holder consisting of a mask clamp and a ring which stretches the backing foil was constructed for this purpose.

The magnetization of the targets has been checked with a sensitive Faraday balance in comparison to unsegmented reference targets of the same mass and evaporation conditions (see Fig. 1). As

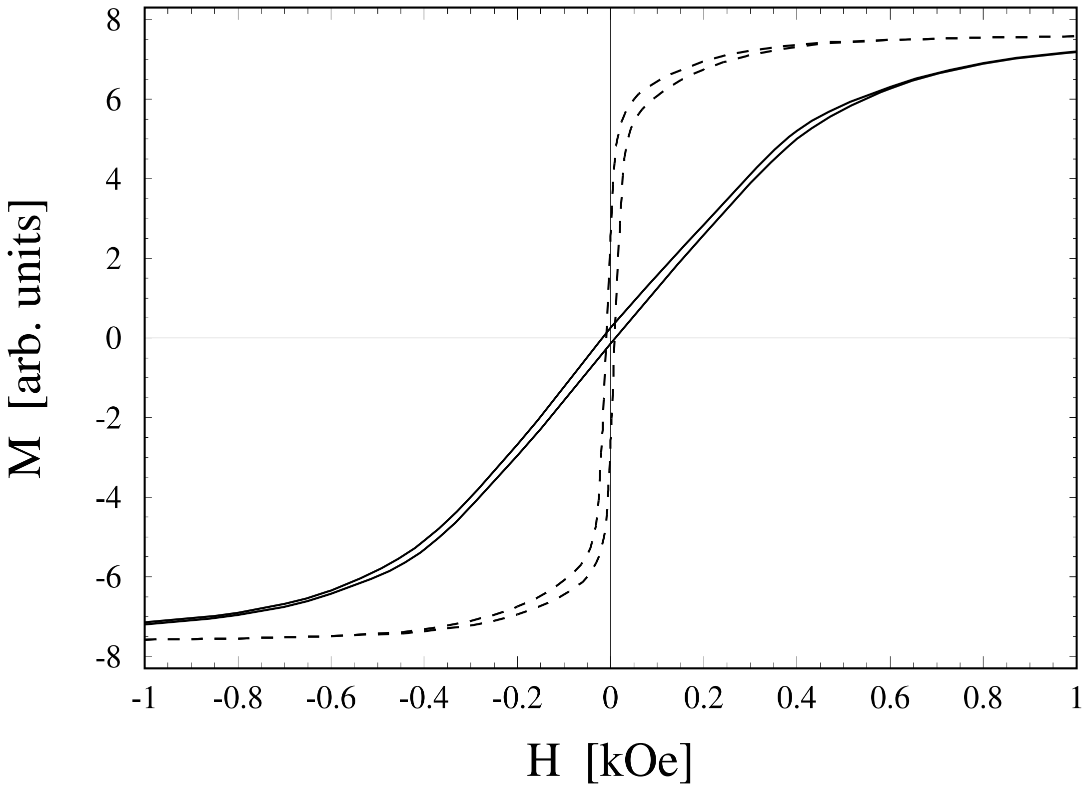

Fig. 1: Magnetization curves for targets with segmented (solid line) and unsegmented (dashed line) iron layer obtained with a Faraday balance

seen in the figure, the segmented targets require external fields of $\geq$ 1 kOe for saturation, whereas 0.5 kOe is sufficient for the unsegmented iron layer.

The production of similar micro-structured targets via the photo-lithographic method is in progress. This technique enables to produce targets with even smaller size of the segments and having perhaps better magnetic properties due to the higher homogeneity and smooth edges of the individual segments.

[1] N. Benczer-Koller et al., Ann. Rev. Nucl. Part. Sci. 30 (1980) 53
[2] K.-H. Speidel et al., Mat. Sci. Forum 97-99 (1992) 615

2.3.5 Development of a discharge plasma target

M. Salvermoser, A. Ulrich, W. Krötz

A discharge plasma target has been developed for laser experiments in the XUV wavelength range [1, 2]. Electrically conducting materials can be evaporated by discharging a 40 kV/ 5 μF capacitor. The target will be used with intense beams from the SIS/ESR facility. High target densities and vacuum outside the excited volume are required for such experiments in order to stop ion beams within a reasonable length and to avoid optical absorption, respectively. Both can be achieved with this type of target.

The setup is schematically shown in Fig. 1. Electrical parameters of the discharge circuit were presented in a GSI-report [3].

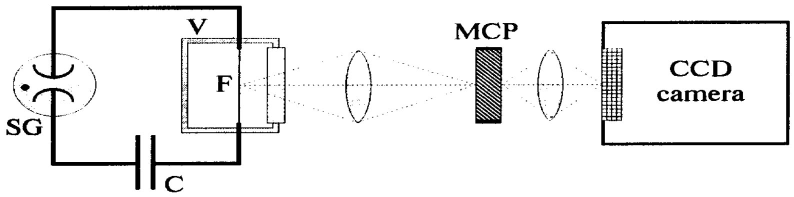

Fig. 1: Setup of fibre target experiments. The discharge circuit with capacitor (C), spark gap (SG), and vacuum chamber (V) with fibre (F) is shown schematically. Optical emission was measured with a CCD-camera, using a gated micro-channel-plate (MCP) as image intensifier.

Meanwhile an image intensified CCD camera is used to study the spatial homogenity of the plasma targets by observing their optical emission. Two-dimensional images of exploding fibres were taken at various times between 0 and 3 μs after the onset of the discharge with exposure times of typically 50 ns. Tungsten fibres are shown in Fig. 2 100 and 800 ns after ignition.

It was possible to determine expansion velocities of plasma columns by analysing images of fibres taken at different times. Velocities of 4 km/s have been measured for copper and 1 km/s for tungsten. The expansion is slowed down and partly controlled by magnetic forces induced by the discharge current.

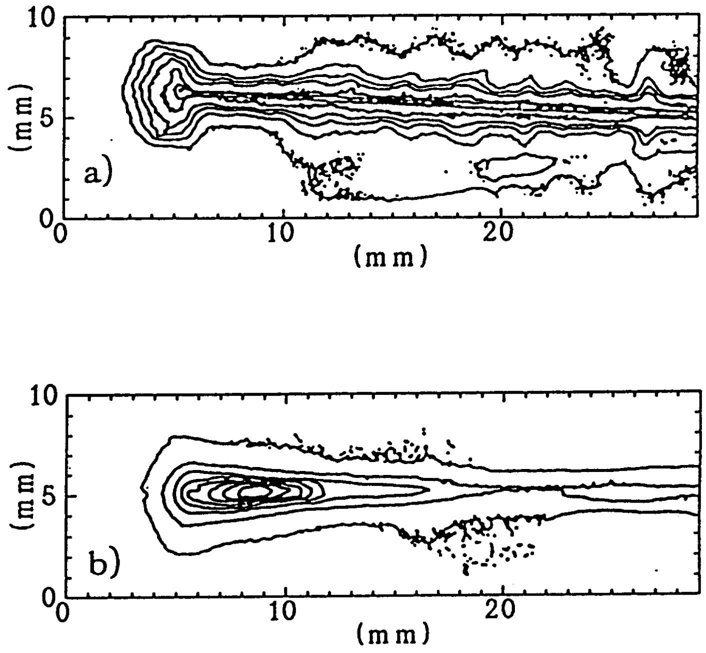

Fig. 2: Images of a 50 mm tungsten fibre 100 ns (a) and 800 ns (b) after ignition. The capacitor was charged to 20 kV. The residual gas pressure was 10^{-3} hPa.

Therefore the plasma columns remained sufficiently stable and spatially homogenious to serve as targets for heavy ion beams up to 2 μs after the onset of the discharge. Particle densities between $5\cdot10^{18}\,\mathrm{cm}^{-3}$ and 10^{20} can be achieved with these targets. At later times the plasma columns get distorted by magnetic instabilities.

Light emitted by the fibre explosion has been analysed spectroscopically and time resolved in the visible spectral range by placing a monochromator in front of the image intensifier. The spectra showed line structures, which could partly be assigned to known transitions of the metal atoms and ions. Line broadening by pressure and Stark effect was also observed.

A new design using tube targets as an alternative to exploding wires was tested to produce carbon plasmas. The tubes were 3.2 cm long and had an inner diameter of 7 mm. The inner wall was covered with a thin (20 $\mu\mathrm{g/cm}^2$) carbon layer. These targets will allow the axes of the tube and the ion beam to coincide. Furthermore this geometry has the advantage, that the discharge current induces a magnetic pressure, which accelerates the implosion in the tube targets, and leads to the formation of a pinch. This could be verified by studying the temporal evolution of these targets and images showing a bright spot near the center of the tube. An analysis of the spectra indicated high temperatures T $\geq$ 26000 K and plasma velocities (v $\approx$ 25 km/s).

Controlling the plasma expansion by an external, pulsed magnetic field from an additional discharge capacitor will be tested in a next step to increase the range of target densities considerably.

[1] R. Miller, Diplomarbeit TUM, 1990
[2] M. Salvermoser, Diplomarbeit TUM 1992
[3] A. Ulrich et al., scientific report 1990 GSI Darmstadt (1991) 425

2.3.6 Heavy ion beam pumped visible laser

A.Ulrich, J. Wieser, A. Brunnhuber, W. Krötz

Heavy ion beam pumped laser action has been observed on the yellow 585.25 nm $3p'[1/2]_0$ - $3s'[1/2]_0^1$ line in NeI. Ternary mixtures of (He, Ne, Ar), (He, Ne, Kr), and (He, Ne, Xe) at a total gas pressure of 790 hPa were pumped with a chopped beam of 120 MeV $^{35}Cl^{9+}$ ions from the Munich Tandem van de Graaff accelerator. The experiment was performed in a program in which heavy ion beam induced emission of light and ion beam pumping of lasers are studied. Infrared laser action had been observed and ion beam induced optical gain was measured on the second excimer continuum of xenon [1] at 172 nm and the 476.5 nm line of ArII [2]. Quasi-continuous laser action well above threshold was now obtained on the 585.25 nm 3p-3s NeI line. This is the heavy ion beam pumped laser with the shortest wavelength, so far.

A specially designed high current ion source which provided Cl-beams up to 100 mA was used for the experiment [3]. The experimental setup of the laser is schematically shown in Fig. 1. It is similar to the setup which had been used for heavy ion beam pumping of infrared lasers [4]. The 585.25 nm NeI laser was first observed in pulsed electrical discharges [5] and recently successfully studied as nuclear pumped laser [6, 7] with parameters similar to those used in the experiment described here.

At laser gas pressures of the order of 10^5 Pa the pumping scheme is complex and dominated by formation and decay of excimer molecules [8]. It is interesting to note that these processes lead to a very selective population of the upper 3p laser level in He-Ne mixtures as indicated by the spectrum

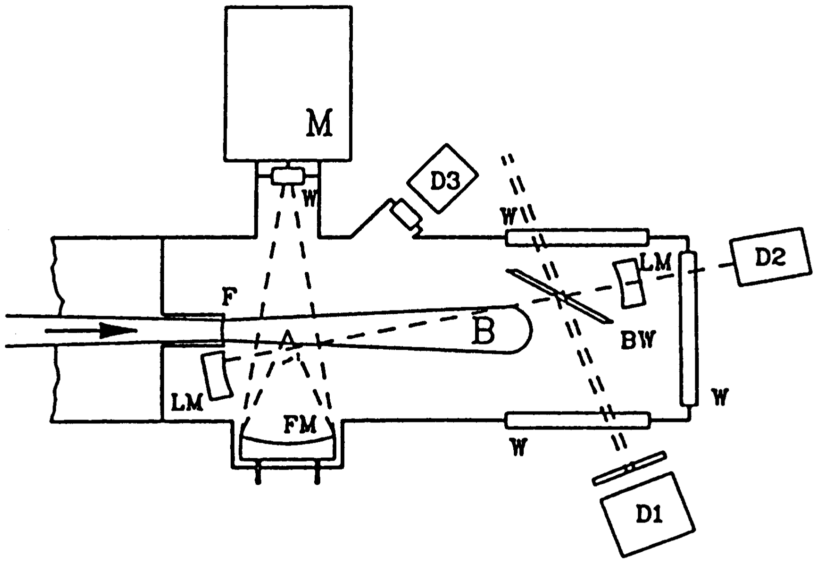

Fig. 1: Schematic drawing of the experimental setup. The ion beam indicated by the arrow enters the laser cell through the entrance foil F. The volume B is pumped by the ion beam. The optical cavity is formed by the laser mirrors LM. Optical windows of the laser cell are indicated by W. A quartz plate approximately at Brewster angle BW is used for output coupling. Laser light is detected with photodiodes D1 and D2. High intensity laser light is attenuated with a neutral density filter in front of detector D1. The photodiode D3 is used for measuring the spontaneous emission of the laser gas. The focusing mirror FM and monochromator M are used for optical spectroscopy of the laser medium.

of the laser gas mixture shown in Fig. 2. Argon, krypton or xenon is added for collisional depopulation of the lower laser level. This compensates for populating of the lower level by resonant photoabsorption from ground state NeI atoms.

The (He, Ne, Ar)-laser gas mixture was optimized by systematic variation of the neon and argon concentration at a fixed helium pressure of 725 hPa. Under the assumption that the Ne and Ar concentrations can be optimized independently the optimum mixing ratio was about 92 % He, 6 % Ne, and 2 % Ar. It was found that the laser gas mixture had to be purified before laser action could be observed. A rare gas purifier with hot titanium was used for that purpose. With an instantaneous pumping power of the ion beam of 500 W the laser output power was 66 mW for the present experimental conditions. This could be substantially improved by using a setup in which the ion beam and laser axis coincide.

Laser action started with beam pulses of more than 2 μs duration. Constant output power was reached after about 3 μs and was observed up to 50 μs after the onset of the beam pulse. Pulse duration was limited by the heating of the 1.1 mg/cm^2 titanium entrance foil of the laser cell. The laser was operated at a repetition rate of typically 50 Hz. Output coupling was varied by rotating the quartz plate which had been installed in the optical cavity for that purpose. Optical gain of 2.6 % and a residual loss of 0.15 % per round trip and 540 mW saturation intensity were determined from a fit to the data obtained from a measurement of the output power versus output coupling.

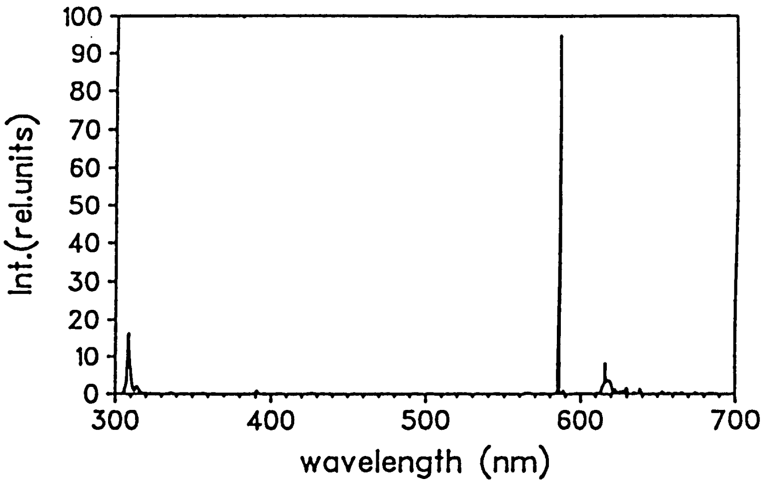

Fig. 2: Emission spectrum of the laser gas mixture

[1] B. Busch et al., scientific report 1991 GSI Darmstadt (1992) 235
[2] J. Wieser et al., scientific report 1991 GSI Darmstadt (1992) 236
[3] A. Brunnhuber, Diplomarbeit TUM 1992
[4] A. Ulrich et al., scientific report 1983 GSI Darmstadt (1984) 156
[5] W.B. Bridges and A.N. Chester, Appl. Optics **5** (1965) 573
[6] E.P. Magda et al., Institute of Technical Physics, Chelyabinsk 70, Russia, internal report
[7] A.M. Voinov et al., 17th Int. Conf. on Quantum Electronics, May 21-25, 1990, Anaheim Cal., USA
[8] E.G. Batyrbekov and V.A. Danilychev, preprint, Kazakh Acad. of Science, Inst. of Nuclear Physics, Alma-Ata 480082, Kazakhstan

2.3.7 Feasibility of an experiment to determine the branching ratio for the emission of a heavy neutrino after muon capture in ^{3}He

W. Schott, V.N. Baturin [a], W.H. Breunlich [b], T. Case [c], H. Daniel, F.J. Hartmann, M. Jeitler [b], P. Kammel [b], K. Lou [d], E.M. Maev [a], J. Marton [b], M. Mühlbauer, C. Petitjean [d], G.E. Petrov [a], Yu.V. Petrov [a], G.G. Semenchuk [a], Yu.V. Smirenin [a], A.A. Vorobyov [a], P. Wojciechowski, J. Zmeskal [b]

[a] St. Petersburg Nuclear Physics Institute, Gatchina, St. Petersburg District 188350, Russia

[b] Österreichische Akademie der Wissenschaften, Institut für Mittelenergiephysik, A-1090 Vienna, Austria

[c] Lawrence Berkeley Laboratory and University of California, Berkeley, CA 94720, USA

[d] Paul Scherrer Institute, CH-5232 Villigen, Switzerland

The triton energy of the muon capture reaction μ^3He $\rightarrow$ t + ν_μ, where μ^3He is the ground state of muonic ^{3}He, has been measured in order to investigate a possible heavy ν admixture into the μ flavour with high sensitivity. μ^3He has been formed via the pμd fusion reaction by stopping μ^- in an ionization chamber filled with an H/D gas mixture of 3 % D concentration at a pressure of 161 bar. In a first short experiment 650 triton events were observed yielding an upper limit for the μ^- heavy ν mixing strength of $2.3 \cdot 10^{-3}$ at $E_{o\nu} = 60$ MeV.

According to the Standard Model, neutrinos (ν) are massless. From the GUT standpoint (Grand Unified Theory) it is more natural for the ν to have mass: ν is a member of a multiplet together with a charged lepton and a positively and a negatively charged quark which all have masses. The present experimental upper limit of the ν_μ rest energy is $E_{o\nu_\mu}$ <0.50 MeV [1]. $E_{o\nu_\tau}$ was measured to be $E_{o\nu_\tau}$ <31 MeV [1]. If the ν decay, the flavour ν eigenstates $\{\nu_\ell\}$ ($\ell = e, \mu, \tau$) can be linear combinations of massive ν eigenstates $\{\nu_i\}_{(i=1,2,3)}$

$$\nu_\ell = \sum_i U_{\ell i} \nu_i \quad ,$$

where U is the neutrino mixing matrix. The upper limit of the admixture into the electron and muon flavour has been determined by looking for oscillations and the decay of ν emitted in reactors and accelerator experiments, respectively. The μ–heavy ν_i mixing strength is $|U_{\mu i}|^2 < 10^{-4}$ for $E_{o\nu_i} >$ 20 MeV [2]. Furthermore, upper limits of $|U_{\mu i}|^2$ were obtained by measuring the μ^+ from the π^+ and K^+ two-body decays into the μ channel $\pi^+ \to \mu^+ + \nu$ for 1 MeV $\leq E_{o\nu} \leq$ 34 MeV and $K^+ \to \mu^+ + \nu$ for 70 MeV $\leq E_{o\nu} \leq$ 388 MeV [3]. The lower boundary of $E_{o\nu}$ is determined by the experimental resolution, the upper boundary by the Q value of the reaction respectively. The μ capture reaction

$$\mu^3 He \to t + \nu \tag{20}$$

was measured for the $|U_{\mu i}|^2$ study by a Louvain-la-Neuve PSI group [4] using a gas scintillation proportional counter with a ^{3}He/Xe gas mixture of 10 % Xe concentration and 5 bar pressure. We (PSI μ CF collaboration) measured the same reaction using the St. Petersburg Nuclear Physics Institute (SPNPI) ionization chamber (IC) where μ^3He was formed via the pμd fusion reaction.

The t kinetic energy T_t of the reaction (eq. 20) is given by

$$T_t = E_{o\mu^3 He} - \sqrt{E_{ot}(2E_{o\mu^3 He} - E_{ot}) + E_{o\nu}^2}.$$

The difference $T_t(E_{o\nu_\mu}) - T_t(E_{o\nu_\mu} = 27\,\text{MeV}) = 0.124$ MeV corresponds to the possible energy resolution (FWHM) of the IC, i.e., the two t lines associated with ν of $E_{o\nu_\mu}$ and 27 MeV rest energies should be separable. $T_t(E_{o\nu} = 86\,\text{MeV}) = 0.63$ MeV is the low energy threshold of the IC yielding the upper limit of the $E_{o\nu}$ range which can be investigated with our detector. $T_t(E_{o\nu} = 105\,\text{MeV} \approx E_{o\mu}) = 0$ is the Q value limit of the reaction (eq. 1). Thus, the $E_{o\nu}$ range covered by our experiment is $27 \leq E_{o\nu} \leq$ 86 MeV filling the gap between the π^+ and K^+ decay experiments.

This measurement was simultaneously the H/D run of the PSI μCF collaboration dt sticking experiment [5] to measure the background below the $\mu\alpha$ line.The setup consists of the IC surrounded by an array of 19 thick plastic n counters with 5.0 sr solid angle and an efficiency for 14 MeV n of 26 % and one liquid NE213 n counter. Five thin plastic e counters between the IC and the n counters with 8.2 sr solid angle and 25 % efficiency act as charged particle veto. The IC anode is subdivided into 19 hexagonal parts of 4 mm width with separate readouts. The IC pulses were analyzed with flash ADCs. μ^- are stopped in the sensitive volume with dimensions x = y = 2 cm in the horizontal plane and z = 1.1 cm in the vertical direction along the electric field. The total probability of μ^3He formation is $P_{\mu^3He} = P_{\mu d} \cdot P_{p\mu d} \cdot P^f_{p\mu d} \cdot P_{p\mu^3He\gamma} = 0.28$ with $P_{\mu d} = 1$, the pμd formation probability $P_{p\mu d} = 0.67$, the pμd fusion probability $P^f_{p\mu d} = 0.49$ and the probability to obtain a 5.2 keV μ^3He and a 5.5 MeV γ after fusion, $P_{\mu^3He\gamma} = 0.85$. One thousandth of the μd form dμd where after fusion most of the μ^- are free for a new cycle. One branch yields a t and a p, another branch a 0.8 MeV μ^3He, both contributing to the background of the μ capture reactions

$$\begin{array}{lcll} \mu^3 He & \to & t + \nu_\mu & (3.3 \cdot 10^{-3}) \\ & \to & d + n + \nu_\mu & (1.3 \cdot 10^{-3}) \\ & \to & p + 2n + \nu_\mu & (3.7 \cdot 10^{-4}) \end{array}$$

with the probabilities denoted in brackets. In one third of the μ capture events the t breaks up into a d and an n or into a p and two n. This breakup d and p are the more serious background events of the t spectrum. Fig. 1 shows a t spectrum obtained after subtracting a constant background and a Gaussian

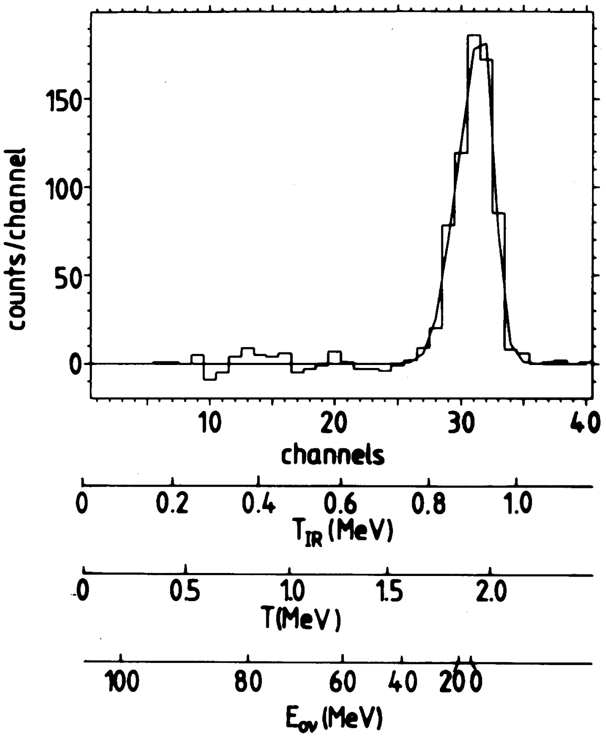

Fig. 1: Triton spectrum after μ^- capture in ^{3}He with a constant background subtracted; T_{IR} means energy including recombination. The drawn line denotes a Gaussian fit. T means real energy, $E_{o\nu}\nu$ rest energy.

fit yielding an energy width dT = 0.19 MeV (FWHM). The observed particle energy T_{IR} which includes the recombination effect of the IC, is smaller than the real energy because some charge is lost due to recombination. The t line contains 650 t events measured in 36.7 h at a mean p current of 120 μA. Fig. 2, curve a, shows the deduced 90% C.L. upper limit of the mixing strength $|U_{\mu i}|^2$ vs. $E_{o\nu}$.
$|U_{\mu i}|^2$ is given by [4]

$$|U_{\mu i}|^2 = \frac{I(E_{o\nu}/I(0)}{\rho(E_{o\nu})/\rho(0)},$$

where $I(E_{o\nu})/I(0)$ is the intensity ratio at $E_{o\nu}$ and zero rest energy, and $\rho(E_{o\nu})/\rho(0) = 0.92...0.32$ for $E_{o\nu} = 30\,\mathrm{MeV}\ldots86\,\mathrm{MeV}$ a corresponding phase factor ratio. Curve b denotes the data of ref. 4. The excluded regions are above curve a and b, respectively. At small $E_{o\nu}$ our $|U_{\mu i}|^2$ measurement is less sensitive than the Louvain-la-Neuve PSI experiment due to the poorer energy resolution of our detector. dT could be reduced by a factor of 1.5. At $E_{o\nu} = 60$ MeV we obtain $|U_{\mu i}|^2 < 2.3 \cdot 10^{-3}$ which corresponds to the $|U_{\mu i}|^2$ sensitivity level with our present statistics if all background events can be suppressed.

The upper limit of $|U_{\mu i}|^2$ can be lowered by

a) Background suppression
b) Intensity increase using an H/^{3}He gas mixture.

The t and breakup d and p particles may be distinguished in the T vs range r plane, where t, d and p lie on different curves. At small T the different pulse shape must be used.

In a planned experiment at PSI using a newly designed IC with a $^3He/H_2$ gas mixture of 130 bar and $c_{H_2} = 0.02$, a t rate of 6 s^{-1} is expected. Since there is no recombination, dT/T = 0.03 can be achieved, thus, making it possible to measure $|U_{\mu i}|^2$ in a two days run at $E_o\nu$ = 18.5 MeV at a level of $7 \cdot 10^{-5}$ with 0.5% breakup background being present. If the background can be suppressed by pulse shape analysis which seems to be possible with the proposed $^3He/H_2$ mixture, the $|U_{\mu i}|^2$ sensitivity would be 10^{-6}.

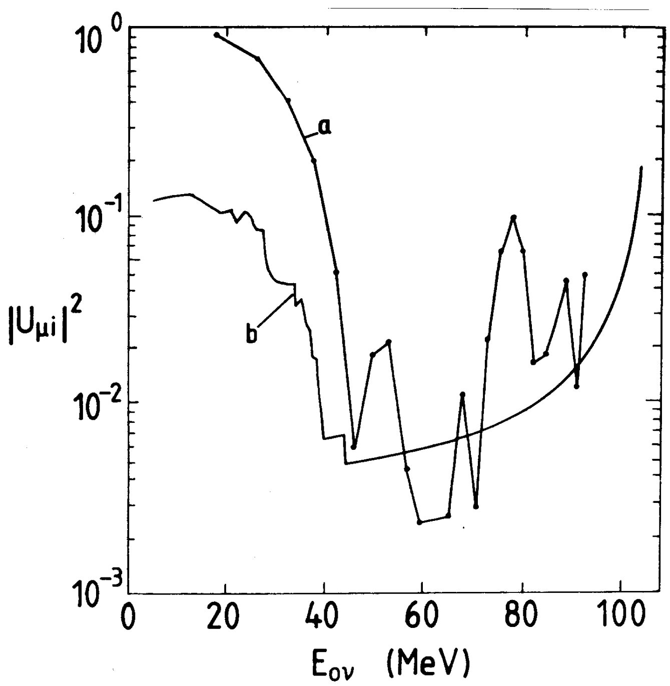

Fig. 2: μ-heavy ν_i mixing strength vs $E_{o\nu}$. (a) This experiment; (b) results of the Louvain-la-Neuve PSI group.

We would like to thank Prof. Dr. J.P. Deutsch and Prof. Dr. S.S. Gershtein for fruitful discussions.

[1] G. Fraser, CERN Courier, 7 (October 1992)

[2] G. Bernardi et al., Phys. Lett. **B166**, 479 (1986)

[3] R. Abela et al., Phys. Lett. **B105** (1981) 263; M. Daum et al., Phys. Rev. **D36** (1987) 2624; R.S. Hayano et al., Phys. Lett. **49** (1982) 1305; Y. Asano et al., Phys. Lett. **104B** (1981) 84; C.Y. Pang et al., **D8** (1973) 1989

[4] B. Tasiaux et al., Part. World **2** (1991) 81

[5] C. Petitjean et al., Muon Catalyzed Fusion **5/6** (1990/91) 261

2.3.8 Measurement of the stopping power for μ^- at energies in the eV range

H. Daniel, F.J. Hartmann, W. Neumann [a], W. Schott
[a] Hauptabteilung für die Sicherheit der Kernkraftwerke, Würenlingen, Switzerland

The spectral flux density n(T) of μ^- emerging from a kapton moderator has been measured at low kinetic energies T using time-of-flight. From n(T) the stopping power S(T) of kapton was determined for 2.5 eV $\leq$ T $\leq$ 750 eV by means of the relation [1] n(T)·S(T) = const. The measured n(T) was corrected for multiple scattering. n(T)·S(T) behind a 0.6 mg/cm^2 thick mylar wedge, a 1.24 mg/cm^2 scintillator and a 0.18 mg/cm^2 kapton foil coated with a 0.05 mg/cm^2 copper sheet was calculated using the stopping power S^a obtained from proton data [2] starting from a Gaussian μ^- distribution in momentum selected by a magnet spectrometer with 8.67 MeV/c in the center and 6 % width (FWHM).

In fig. 1 the resulting S vs. T values and the S^a(T) curve scaled to the corresponding μ^- velocity, are plotted. At larger T S agrees fairly well with S^a, whereas at small T, S is more than two orders of magnitude smaller than the extrapolated S^a indicating that the absorption of μ^- is very small in this T range [3].

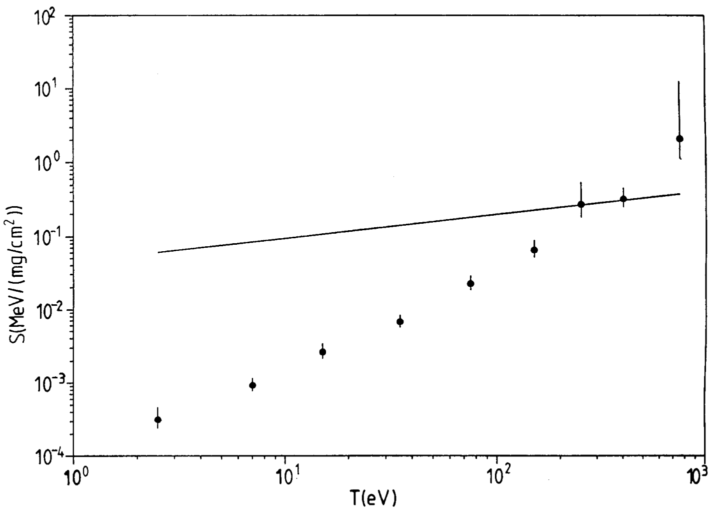

Fig. 1: Stopping power S of kapton vs. μ^- energy T. The drawn lines represent S^a values.

[1] G. Fottner, H. Daniel, P. Ehrhart, H. Hagn, F.J. Hartmann, E. Köhler and W. Neumann, Z. Phys. **A304** (1982) 333
H. Daniel, Biol. Trace Elem. Research **13** (1987) 301

[2] J.F. Ziegler, J.P. Biersack and U. Littmark, The Stopping and Range of Ions in Solids, New York: Pergamon Press 1985

[3] H. Daniel, Phys. Rev. Letters **35** (1975) 1649
H. Daniel, Phys. Rev. **A15** (1977) 1338

2.3.9 Frictional cooling – a new approach in phase space compression at low particle energies

M. Mühlbauer, H. Daniel, F.J. Hartmann

Positive as well as negative slow muons are often used as probes in surface and thin-film physics. Experiments on gas targets, especially in muon-catalyzed fusion research, are very important too [1]. Slow muons are normally produced by moderation of high-energy muons from pion decay. New developments are the extraction of slowed down muons from an anticyclotron [2] and the conversion of muons via the muon-catalyzed dt-fusion cycle [3]. All these methods do not yield a muon beam with a narrow energy distribution, high intensity and high density in phase space. Of course, one can increase the intensity by increasing the intensity of the primary beam used for pion production, but there are much more efficient ways. Density in phase space can be increased by cybernetic cooling, for example using the so-called 'phase space compression' device (PSC) [4]. A less complicated way was calculated to be available by cooling a charged particle beam by moderation in matter and simultaneous acceleration in an electrostatic field, the so called frictional cooling [1].

Basic Idea: Frictional cooling is based on the fact that the stopping power S of matter,

$$S = -\frac{\mathrm{d}T}{\mathrm{d}s} \tag{21}$$

with s = pathlength, increases with the particle energy T for particles at low T, $T \lesssim 10\,\mathrm{keV}$ for muons as shown in fig. 1 and $T \lesssim 100\,\mathrm{keV}$ for protons. Under these conditions the energy loss per pathlength s is greater for particles moving at higher energies than for particles at lower energies. An applied electrostatic field $\vec{E}$, $|\vec{E}| = E$, along the beam axis compensates for the energy loss. This electric field defines an equilibrium energy T_{eq},

$$S(T_{\mathrm{eq}}) = qE, \tag{22}$$

in a way that the energy loss of a particle due to the stopping power is equal to the energy gain of a particle with charge q under the influence of the electrostatic field. Under these conditions particles with $T > T_{\mathrm{eq}}$ will be decelerated — they loose more energy than they gain. On the other hand particles with $T < T_{\mathrm{eq}}$ will be accelerated. The electric field acting along the beam axis compensates only for the energy loss in beam direction and not for the energy loss perpendicular to it. Both longitudinal motion different from the equilibrium velocity v_{eq} corresponding to T_{eq} and transversal motion die out exponentially with time. The time constant is independent of the particle velocity [1, 7, 8]. Therefore we obtain an increase in spectral density and a decrease in beam divergence and the effects of multiple scattering and straggling will simultaneously be strongly reduced.

Expected Results: The feasibility of a frictional cooling device was studied by closed-form calculations and by detailed Monte Carlo simulations [7, 8]. Large-angle scattering, straggling and the exact field distribution inside an accelaration tube were taken into account. The influence of a strong axial magnetic field on beam dimension and volume in phase space was investigated. The calculations were performed for slow muons in a gaseous hydrogen moderator and in a setup of many thin (a few $\mu\mathrm{g/cm}^2$) carbon foils.

Closed-form calculations and Monte Carlo simulations for the hydrogen setup indicate that a low-energy charged-particle beam can be compressed in energy by frictional forces. As shown in fig. 2 the spectral density will be improved by a factor of 6 to 9, yielding a width of the energy distribution $\sqrt{\langle \Delta T^2 \rangle}$ of 0.3 keV to 0.6 keV depending on the equilibrium energy defined by the acceleration field. The beam divergence of the outgoing muons was found to be small (see fig. 2) and independent of the

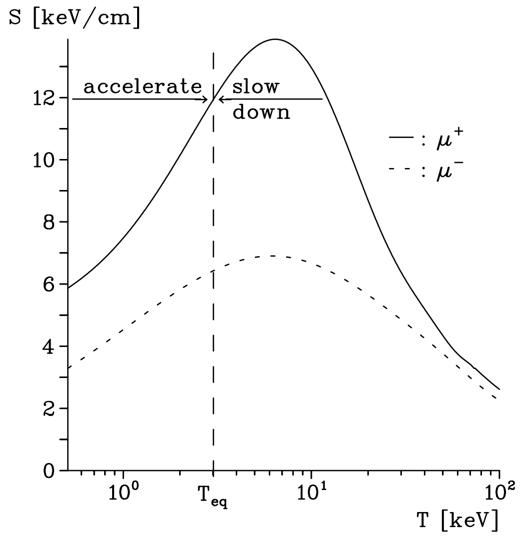

Fig. 1: Average stopping power $S(T)$ of H_2 at 40 mbar for μ^+ (scaled proton data from Janni [5]) and μ^- (data from Hauser et al. [6]); $T_{\rm eq}$ denotes the equilibrium energy.

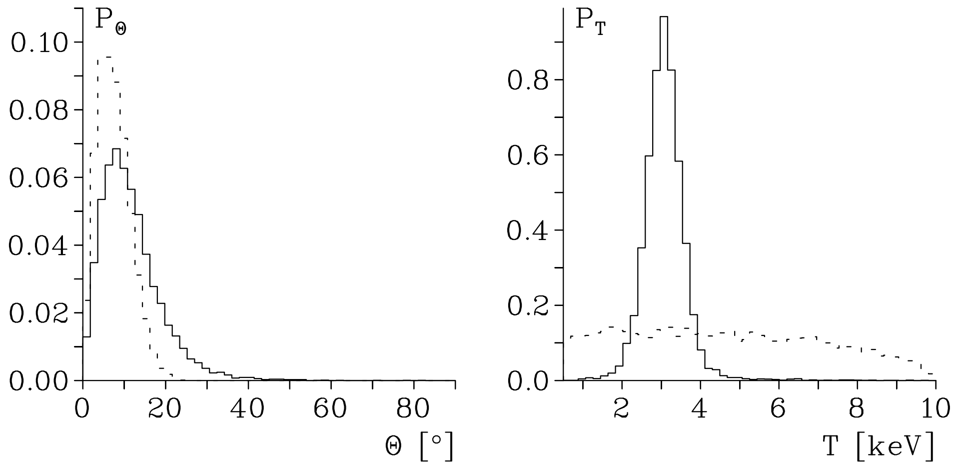

Fig. 2: Angular and energy distribution P_Θ and P_T, respectively, of incoming (- - -) and outgoing (—) muons; hydrogen moderator; $T_{\rm eq} = 3$ keV; muon source with small angular distribution.

beam divergence of the incoming muons. As expected, we obtain an increase of the mean equilibrium angle and also an increase of the width of the angular distribution for a decreasing equilibrium energy. Nevertheless we obtain a smaller energy distribution and therefore a greater gain in spectral density for a lower equilibrium energy because of the larger gradient of the stopping power at lower energies. The beam diameter, which is increasing according to the beam divergence, can be conserved by a strong axial magnetic field which guides the muons on spiral orbits along the magnetic field lines. In case of a realistic beam as shown in fig. 3 with a spot size of about 20 cm and a divergence according to Lambert's law (cosine-distribution) the simulations show that the density in phase space (five dimensions) can be increased by up to a factor of 60. There is no need of a focussing magnetic field in this case, because of the great diameter of the incoming beam. The compression is achieved within a short 'distance' of 50 to

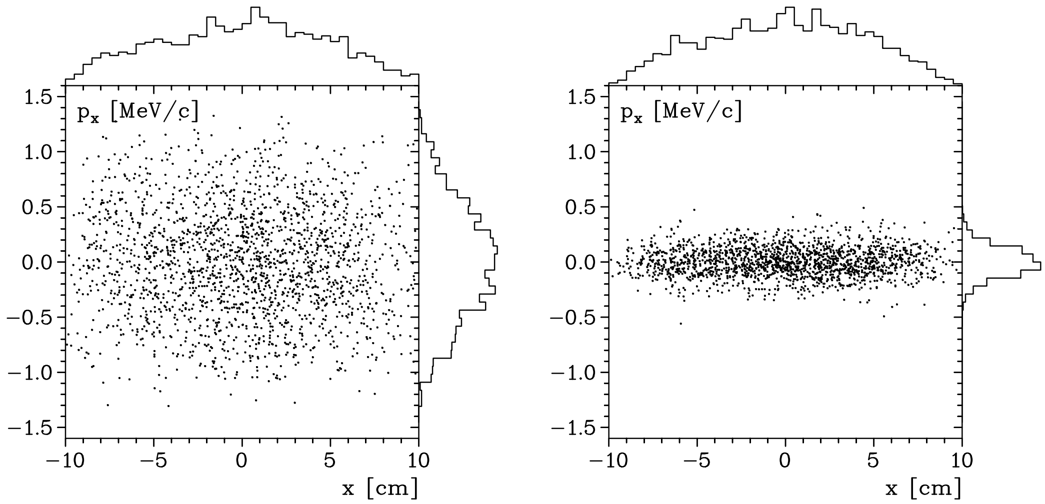

Fig. 3: Phase space diagramm (plane (x, P_x))) of incoming (left) and outgoing (right) muons; hydrogen moderator; $T_{\rm eq} = 3$ keV; muon source with an angular distribution according to Lambert's law.

$100\,\mu$g/cm^2 of moderator material. Large-angle scattering gives only a small deterioration. Only a few percent of the muons are lost.

If instead of gaseous hydrogen thin carbon foils are used as moderator, the simulations yield similar results. According to the higher atomic number, the increase in spectral density and density in phase space is found to be smaller and a larger fraction of the muons is lost.

Summary and Outlook: Calculations and the Monte Carlo simulation indicate that a low-energy charged-particle beam can be compressed in energy by frictional forces. First experiments with slow muons in a hydrogen moderator will be done within the framework of the next Munich-PSI-ETHZ stopping power experiment [9] in early spring 1993.

This work was supported by the German BMFT.

[1] H. Daniel, Muon Catalyzed Fusion **4** (1989) 425.

[2] L.M. Simons , Phys. Bl. **48** (1992) 261. Cf. also H. Daniel, Nucl. Instr. Meth. **24** 1963) 181; Z. Phys. **A313** (1983) 249; LA-UR 84-3248 (1984).

[3] P. Strasser et al., *Int. Conf. Muon Catalysed Fusion*, Uppsala, Schweden (June 28$^{\rm th}$ – July 3$^{\rm rd}$ 1992), to be published.

[4] D. Taqqu, Nucl. Instrum. Methods **A274** (1986) 288.

[5] J.F. Janni, At. Data Nucl. Data Tables **27** (1982) 147.

[6] P. Hauser et al., *Int. Workshop on Muonic Atoms and Molecules*, Ascona, Switzerland (April 5$^{\rm th}$ – 9$^{\rm th}$, 1992), proc. Birkhäuser Basel (1993).

[7] M. Mühlbauer et al., ibidem.

[8] M. Mühlbauer, diploma thesis, Tech. University of Munich, 1992, unpublished.

[9] P. Wojciechowski et al., this Jahresbericht.

2.3.10 Measurement of the stopping power for μ^- and μ^+ at energies between 3 keV and 80 keV

P. Baumann, H. Daniel, A. Fuchs [a], F.J. Hartmann, P. Hauser [a], F. Kottmann [b], K. Lou [a], M. Mühlbauer, C. Petitjean [a], W. Schott, D. Taqqu [a], P. Wojciechowski
[a] Paul Scherrer Institut, CH-5232 Villigen PSI, Switzerland
[b] Institut für Hochenergiephysik, ETH Zürich, CH-8093 Zürich, Switzerland

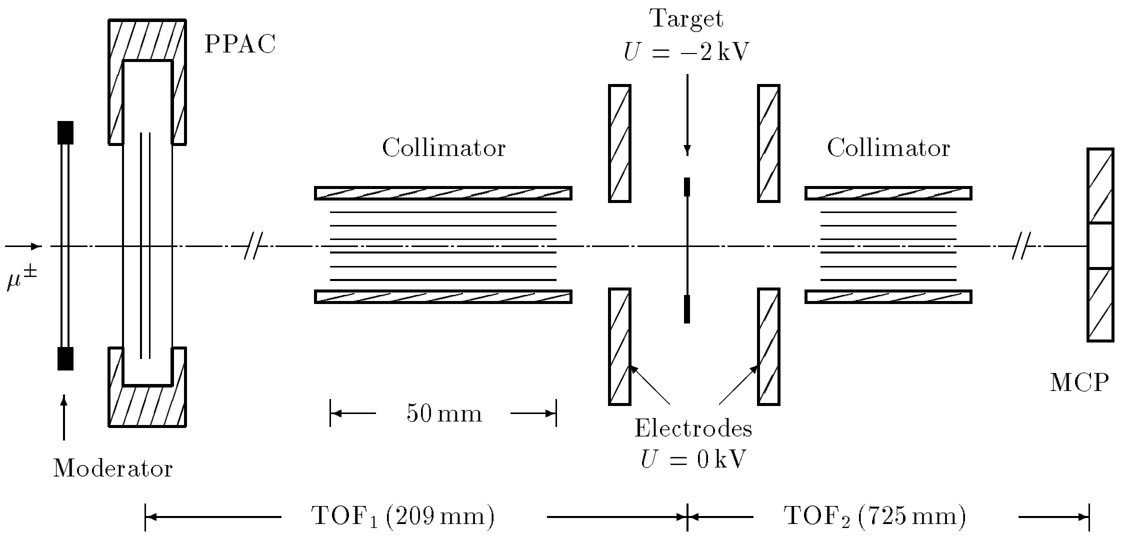

Fig. 1: Schematic view of the experimental setup showing both time-of-flight (TOF) sections. The Wien filter, the quadrupoles in front of the setup and the solenoid generating a field in beam direction are not shown. The cross-section of moderator, PPAC foils and collimators perpendicular to the beam axis is square, whereas that of electrodes, target foil and MCP is circular. For further explanations see text.

The Experiment: An experiment has been performed in the πE1 area of PSI in spring 1992 in order to measure the stopping power S of carbon, gold and magnesium fluoride for μ^- and μ^+ at energies between 3 keV and 80 keV. Such an experiment seemed very desirable because there exist only very little data on the stopping power for slow heavy negative particles [1,2] and hence also on the Barkas effect [3,4]. The great advantage performing the measurements at PSI lies in the possibility to switch between particles and their antiparticles within a couple of minutes. Another aim of the experiment was to study the feasibility of new phase-space-compression techniques based on frictional cooling of charged particle beams [5,6].

For the measurements part of the existing device for phase space compression (PSC) of muons was used [7]. The setup is shown in Fig. 1. S can be derived from the energy loss $\Delta T = T_2 - T_1$ of the muons in the target and from the thickness of the target. Here T_1 and T_2 denotes the kinetic energy before and behind this target, respectively. T_1 and T_2 were determined from their respective time-of-flight (TOF). The first start signal came from a parallel plate avalanche counter (PPAC). The target foil was at the end of the first and the beginning of the second TOF section. At the end of the second section a microchannel plate detector (MCP) was located. The muons crossing the target lost part of their energy and ejected secondary electrons that were accelerated because the target was held at a negative high voltage. The electrons reached the MCP prior to the muons and provided the stop signal for the first TOF measurement and simultaneously the start signal for the second one. The signal in the MCP from the muon, finally, stopped the second TOF measurement.

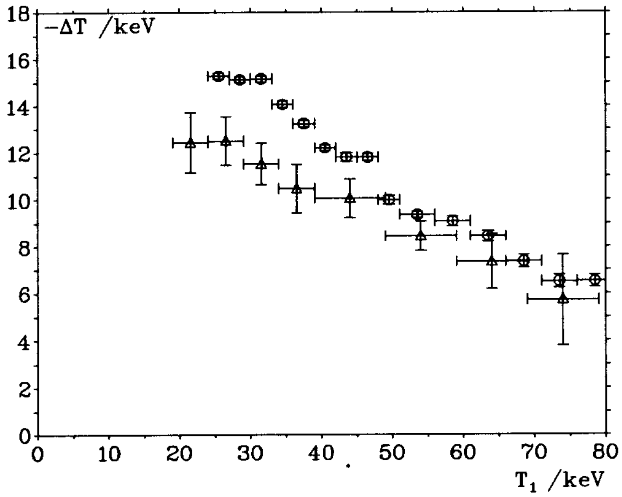

Fig. 2: Energy loss ΔT vs. kinetic energy T_1 for negative (triangles) and positive (circles) muons in a carbon target with a thickness of $21\,\mu g/cm^2$. Only the statistical errors are shown for ΔT. The bars in T_1 direction indicate the T_1 range for the corresponding data point.

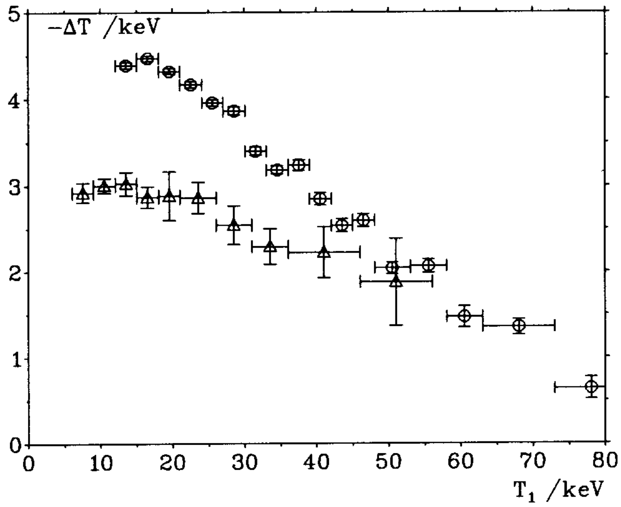

Fig. 3: Energy loss ΔT vs. kinetic energy T_1 for negative (triangles) and positive (circles) muons in a carbon target with a thickness of $5.0\,\mu g/cm^2$. (See Fig. 2 for further details.)

A superconducting solenoid surrounded that part of the setup which is visible in Fig. 1. The use of this solenoid was essential, as its magnetic field (typically 3 Tesla) made the diverging muons spiral around the field lines and directed them onto target and MCP. Depending on the divergence the particles have nonvanishing transverse momentum. In order to minimize the resulting uncertainty of the measurement a collimator was placed in front of the target and behind it, respectively. These collimators consisted of stacks of parallel plastic foils (thickness 0.1 mm) with a distance of 3 mm or 1.5 mm between the foils and a length of 50 mm and 30 mm in beam direction, respectively.

First Results: The energy loss ΔT was measured for different target thicknesses and materials. Figure 2 shows ΔT for μ^- and μ^+ in a carbon target with a thickness of $21\,\mu g/cm^2$. This target was suitable to measure ΔT especially for higher energies where S is small. In the lower energy region the data points for μ^+ lie above those for μ^-. This indicates an increase of the Barkas effect with decreasing energy. Figure 3 gives the results from our measurements of ΔT in a $5\,\mu g/cm^2$ carbon target. As this target was

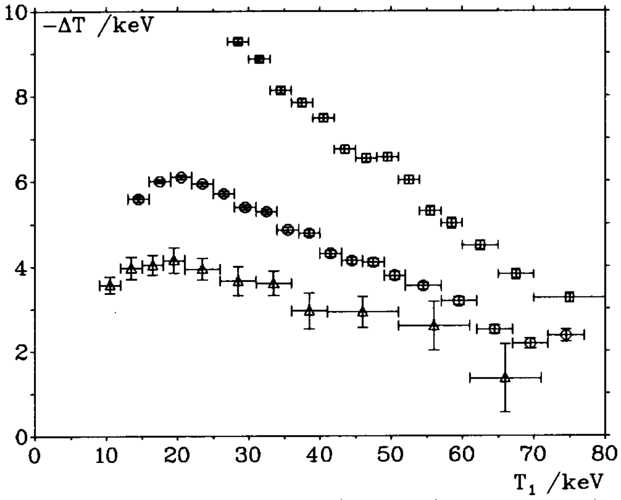

Fig. 4: Energy loss ΔT vs. kinetic energy T_1 for negative (triangles) and positive (circles) muons in a gold target with a thickness of 20 μg/cm^2 on a carbon backing (thickness 3.5 μg/cm^2). ΔT for positive muons in a MgF_2 target (squares) with a thickness of 10 μg/cm^2 on a carbon backing (thickness 4.5 μg/cm^2) is also shown.

fairly thin, it provided ΔT data down to very low energies and the Barkas effect is clearly seen. Almost no data could be taken for μ^+ from some keV below the Bragg maximum downward. The reason for this may be that for low energies the probability of muonium formation in the target becomes significant. Muonium is neutral and not guided to the MCP by the magnetic field. In Fig. 4 ΔT for gold (μ^- and μ^+) and MgF_2 (only μ^+) can be found.

The results shown here are preliminary as they were extracted from the raw data and neither corrected for beam divergence nor for the influence of the carbon backings. The detailed data analysis will improve the measured absolute stopping power values. It is not expected, however, that the observed stopping power difference between μ^- and μ^+ will be significantly affected.

Outlook: In 1993 we hope to get better statistics, especially for μ^-. In order to show the Z dependence of the energy loss for muons, measurements with a hydrogen gas target and some other materials such as Si and Ti are planned. Furthermore first tests on the stopping in a very low density hydrogen target will extend the range of the stopping power measurements to the lowest energies (below 1 keV). It will also allow to test new possibilities for laser spectroscopy of the μp atom [8] together with first studies of frictional cooling [6].

Acknowledgements: We wish to thank the PSI crew and Dr. P. Maier-Komor, K. Nacke, H. Angerer, M. Aigner and H. Grünwald of the Technische Universität München for their very valuable help. Financial support by the German Bundesministerium für Forschung und Technologie is acknowledged.

[1] W. Wilhelm, H. Daniel and F.J. Hartmann, Phys. Lett. **98B** (1981) 33.
[2] R. Medenwaldt, S.P. Møller, E. Uggerhøj, T. Worm, P. Hvelplund, H. Knudsen, K. Elsener and E. Morenzoni, Nucl. Instr. Methods **B58** (1991) 1.
[3] W.H. Barkas, W. Birnbaum and F.M. Smith, Phys. Rev. **101** (1956) 778.
[4] W.H. Barkas, N.J. Dyer and H.H. Heckman, Phys. Rev. Lett. **11** (1963) 26.
[5] H. Daniel, Muon Catalyzed Fusion **4** (1989) 425.
[6] M. Mühlbauer et. al., this Jahresbericht.
[7] D. Taqqu, Nucl. Instr. Methods **A247** (1986) 288.
[8] D. Taqqu, PSI Letter of intent R–93–04.0.

2.3.11 Long-lived antiprotonic helium atoms: formation in helium gas and quenching by H_2

T. Yamazaki [a], E. Widmann [a], I. Sugai [a], R.S. Hayano [b], M. Iwasaki [b], S.N. Nakamura [b], K. Shigaki [b], H. Tamura [b], A. Kawachi [b], T. Ito [b], H. Daniel, F.J. Hartmann, J. Hoffmann, P. Hofmann, Y.S. Kim, W. Schmid, T. von Egidy, N. Nishida [c], W. Higemoto [c], Y. Ito [d], N. Morita [e], J. Eades [f]

[a] Institute for Nuclear Study, University of Tokyo, Japan

[b] Department of Physics and Meson Science Laboratory, University of Tokyo, Japan

[c] Tokyo Institute of Technology, Japan

[d] Research Center for Nuclear Science and Technology, University of Tokyo, Japan

[e] Institute for Molecular Study, Okazaki, Japan

[f] CERN, Geneva, Switzerland

The exotic-atom cascade normally proceeds very fast (within picoseconds) by radiative transitions, by internal (and external) Auger effect and by Stark mixing. As early as in 1964 Condo [1] suggested, however, that the decay characteristics of negative (π^- and K^-) mesons in helium bubble chambers could be explained by the capture of these particles in large-angular-momentum metastable states of exotic helium atoms. Russell [2] predicted that similar atoms might be formed by antiprotons in liquid helium. Two decades later the postulated metastability of K^- and π^- mesonic atoms was corroborated by experiment [3-5] and very recently it was observed [6] that $\approx$ 3% of the antiprotons stopped in liquid helium survive for several μs before annihilating with the helium nucleus. This is roughly a million times longer than the typical lifetimes of antiprotons that come to rest in matter and it presents a signature for the for the formation of metastable antiprotonic helium atoms. In 1992 an experiment was performed at LEAR of CERN to find out if the same phenomenon may be observed in gas-phase helium.

The monoenergetic $\overline{\mathrm{p}}$ beam of 100 MeV/c momentum (5.6 MeV kinetic energy) traversed a 100 μm plastic scintillator before entering a vessel containing helium gas, where almost all the $\overline{\mathrm{p}}$ stopped. Charged mesons resulting from $\overline{\mathrm{p}}$ annihilation were detected by scintillation counter arrays almost entirely surrounding the stopping area. The time delay between the $\overline{\mathrm{p}}$'s arrival in the gas and its annihilation was digitized. It was very important to minimize the detection inefficiency of the beam scintillator, as undetected antiprotons may follow a given antiproton within the time range of interest, and produce fake delayed events. We only accepted annihilation events in which three charged particles were recorded simultaneously in the scintillation counter arrays. This requirement eliminated events of 2.2 μs mean lifetime caused by $\pi^+ \to \mu^+ \to e^+$ decay by prompt annihilation.

Figure 1a shows time spectra of $\overline{\mathrm{p}}$ annihilation in ^{4}He gas (3 atm), ^{3}He gas (3 atm) and liquid ^{4}He. Fraction and spectral shape of the delayed component were almost the same in the gas at pressures between 2 and 10 atm and in the liquid. This contradicts the hypothesis of collisional excitation or deexecitation of the metastable atom in pure helium.

The spectra shown in Fig. 1a cannot be represented by a simple analytical expression. Therefore an average lifetime was defined by

$$t_{\mathrm{av}}(> t_0) = \frac{\int_{t_0}^{50\mu s} t\, n(t)\,\mathrm{d}t}{\int_{t_0}^{50\mu s} n(t)\,\mathrm{d}t} \tag{23}$$

with t_0 an initial time. The average annihilation time for $\overline{\mathrm{p}}$ in ^{3}He is (15 ± 2)% shorter than in ^{4}He. A crude estimate [7] indicates that the overall cascade time is proportional to the square of the reduced mass of the antiproton, which differs by 7% between ^{3}He and ^{4}He.

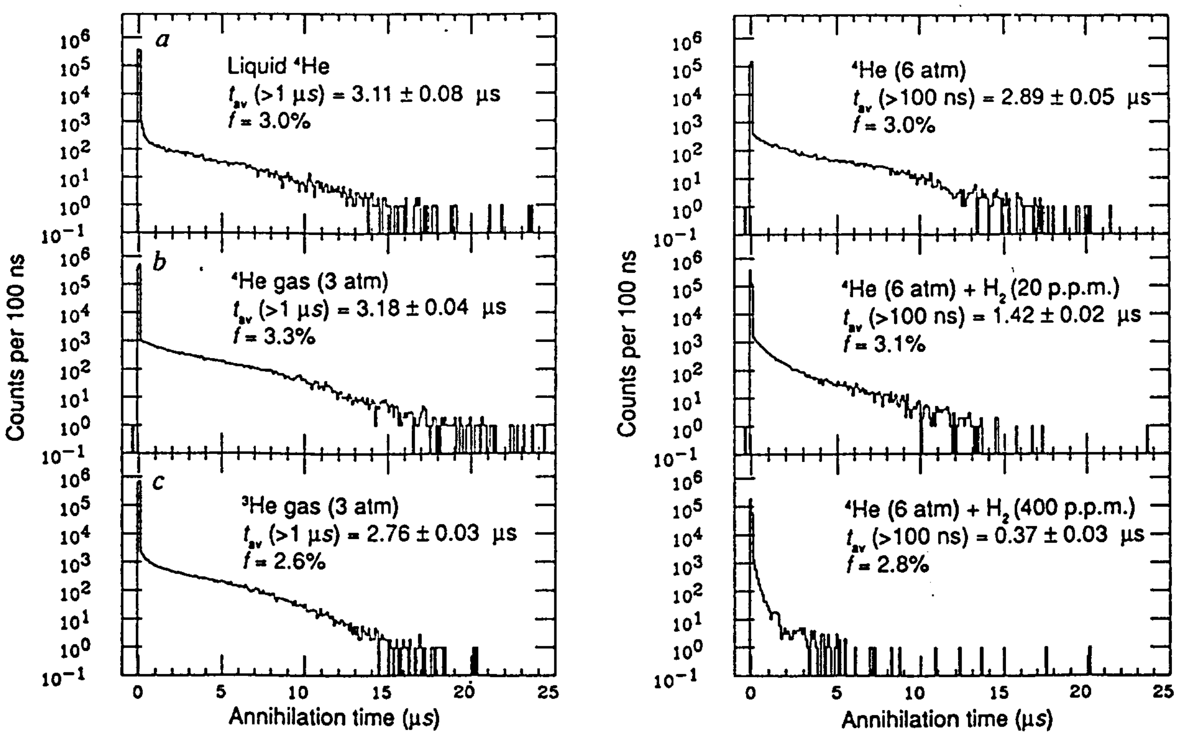

Fig. 1: Time spectra of $\overline{\mathrm{p}}$ annihilation in pure helium and in helium with hydrogen admixtures. The typical values for $t_{\rm av}(> t_0)$ for $t_0 = 1\mu$s and the delayed fraction f are shown in the graphs.
a) Annihilation time spectra from liquid helium (upper), ^{4}He gas (middle) and ^{3}He gas.
b) The effect of hydrogen gas impurities on the metastability of $\overline{\mathrm{p}}$-He.

As can be seen from Fig. 1b, the time spectrum of delayed annihilations is rather sensitive to small admixtures of hydrogen. Already at hydrogen concentrations as small as 20 ppm a sizable effect is seen and at concentrations of 400 ppm the lifetime is reduced to 0.37 μs. The effect is roughly the same for oxygen but far less pronounced for nitrogen. Admixture of a noble gas of low atomic number (Ne or Ar) gives nearly no quenching, whereas noble gases of high Z (Kr or Xe) are much more efficient in quenching the metastable states. All foreign admixtures leave the fraction of metastable $\overline{\mathrm{p}}$-He atoms unchanged. This indicates that the $\overline{\mathrm{p}}$-He formation process is unchanged by admixtures and collisions *after* formation lead to quenching.

[1] G.T. Condo, Phys. Lett. **9** (1964) 65.
[2] J.E. Russell, Phys. Rev. Lett. **23** (1969) 63; Phys. Rev. **188** (1969) 187; Phys. Rev. **A1** (1970) 721.
[3] T. Yamazaki et al., Phys. Rev. Lett. **63** (1989) 1590.
[4] S.N. Nakamura et al., Phys. Rev. **A45** (1992) 6202.
[5] R.S. Hayano, M. Iwasaki and T. Yamazaki, Perspectives of Meson Science, edited by T. Yamazaki and K. Nagamine, p. 417 (North Holland, Amsterdam, 1992).
[6] M. Iwasaki et al., Phys. Rev. Lett. **67** (1991) 1246.
[7] T. Yamazaki and K. Ohtsuki, Phys. Rev. **A45** (1992) 7782.